


Spin-Orbit Effects on Exciton Complexes in Diamond

Shinya Takahashi,¹ Yoshiki Kubo,¹ Kazuki Konishi,¹ Riadh Issaoui,² Julien Barjon³, and Nobuko Naka^{1,*}¹Department of Physics, Kyoto University, Kitashirakawa-Oiwake-cho, Sakyo-ku, Kyoto 606-8502, Japan²LSPM-CNRS, Université Sorbonne Paris Nord, 99 Avenue Jean-Baptiste Clément, 93430 Villetaneuse, France³GEMaC, Université de Versailles St-Quentin-en-Yvelines, CNRS, Université Paris-Saclay,

45 avenue des États-Unis, 78035 Versailles cedex, France

 (Received 21 August 2023; revised 24 November 2023; accepted 20 January 2024; published 26 February 2024)

Ultrafine splittings are found in the optical absorption spectra of boron-doped diamond measured with high resolution. An analytical model of an exciton complex is developed, which permits assigning all absorption lines and sizing the interactions among the constituent charges and crystal field. We conclude that the entry of split-off holes in the acceptor-bound exciton fine structure yields two triplets separated by a spin-orbit splitting of 14.3 meV. Our findings thereby resolve a long-standing controversy [R. Sauer *et al.*, Revised fine splitting of excitons in diamond, *Phys. Rev. Lett.* **84**, 4172 (2000).; M. Cardona *et al.*, Comment on “Revised fine splitting of excitons in diamond,”, *Phys. Rev. Lett.* **86**, 3923 (2001).; R. Sauer and K. Thonke, Sauer and Thonke reply, *Phys. Rev. Lett.* **86**, 3924 (2001).], revealing the underlying physics common in diverse semiconductors, including diamond.

DOI: 10.1103/PhysRevLett.132.096902

Spin-orbit interaction arises from the relativistic effect of the spin angular momentum on valence electron orbitals, and its strength Δ varies with the atomic number z as $\Delta \propto z^4$. It is the basis for spintronics [1,2] and various exotic concepts in solids and ultracold atoms, e.g., topological supersolids and quartet superfluids under artificial gauge fields [3,4]. Combined with spin exchange interaction, it determines the energy structures of optical centers, formed around defects in a crystal lattice, and excitons, which are Coulomb-bound pairs of an electron and a hole. These energy structures critically impact the quantum emission yields [5–7] and spin readout fidelity of quantum sensors [8] formed of organic and inorganic crystals.

In analogy with the deuteron theory in nuclear physics [9,10], the energy structures of excitons in semiconductors have been thoroughly investigated in terms of hole-hole *spin* exchange interaction on top of crystal-field interaction for more than 50 years [11–15]. However, the spin-orbit effect on excitons is not observed in classical semiconductors, such as silicon, germanium, and gallium arsenide, which have narrow band gaps with cubic crystal structures. This is because the excessively large spin-orbit coupling of heavy atoms expels the split-off hole band, arising from the spin-orbit interaction, out of the excitonic fine structure of the smaller splitting. Contrastingly, the split-off hole band for excitons in wide-band-gap wurtzite-type semiconductors has been extensively considered [16–18]. Therefore, a large gap remains in the understanding between the two groups of semiconductors at the opposite extrema on the energy scale.

In this study, we investigated the fine structures of acceptor-bound excitons in diamond by considering the

split-off characteristics of holes. We established a unified model of exciton complexes in semiconductors including silicon based on current industrial relevance and emerging materials for next-generation technologies where excitons dominate at room temperature. We used diamond, a key elemental semiconductor for low-consumption power devices and quantum technologies [8], to fill this gap, which has become important with the emergence of excitonics in two-dimensional materials [19,20] and exciton Rydberg physics [21,22]. Counterintuitively, the small spin-orbit coupling of light carbon atoms is ideal for exploring the role of split-off holes on excitons [23,24], whose responses appear ~ 0.1 eV below the indirect band gap of diamond at 5.5 eV [25,26].

Here we deal with a dopant site occupied by one exciton—an impurity-bound exciton. Theoretically, impurity-bound excitons are understood based on spin coupling of two particles of the same charge and an oppositely charged particle localized around the impurity potential [Fig. 1(a)]. When the impurity is an acceptor (e.g., boron in silicon), the model approximates the four-body bound state

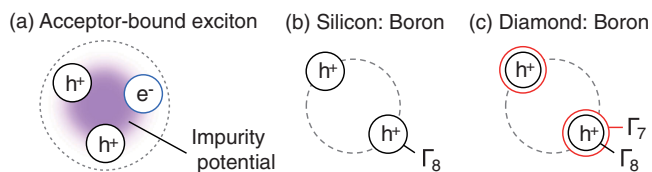


FIG. 1. (a) Four-body diagram of an acceptor-bound exciton, (b) conventional model describing an acceptor-bound exciton, considering only Γ_8 acceptor holes, and (c) our model introducing the split-off holes of Γ_7 symmetry.

by considering the coupled states of the two holes in the top acceptor level [Fig. 1(b)]. The two holes reside in antisymmetric spin states with two different total angular momenta (J), reflecting their fermionic character. One of the J states further splits into two manifolds in the crystal field (exhibiting a symmetry lower than spherical), yielding a *triplet* bound-exciton structure in cubic semiconductors [11]. Experimentally, the triplet structure was decisively established for excitons bound to acceptors in silicon [12]. This crystal-field scheme based on two-hole states is the standard model for bound excitons in semiconductors [13–15].

Although diamond possesses cubic structure similar to silicon, the cathodoluminescence spectrum of boron-doped diamond exhibited a double quadruplet instead of a triplet [27,28]. This observation, made 20 years ago, has excluded diamond from the common understanding of semiconductor physics, resulting in the strong ongoing debate [28–30]. The experimental challenges lie in the absence of absorption measurements on the bound exciton in diamond until recently, owing to the lack of appropriately doped samples [31]. Here, we report extra fine splittings found by improved spectral resolution, which support our crystal-field scheme including the split-off hole [red circles in Fig. 1(c)]. This closes the debate by demonstrating a unified description of the spin-orbit interaction in exciton complexes in semiconductors, as explained below.

Referring to the original crystal-field scheme [12], we used group theory to treat the energy levels in boron-doped diamond. The top valence band of diamond comprises two levels separated by approximately 6 meV through spin-orbit interaction [32]. After doping boron atoms at substitutional sites with carbon atoms, the symmetry is lowered to cubic without inversion [33]. Doping induces the formation of acceptor levels at approximately 360 meV above these valence bands. Reflecting the valence band splitting, the weakly bound hole of the acceptor splits into two levels with a reduced separation of 2 meV [Δ_a in Fig. 2(a)], as measured by electronic Raman spectroscopy [34] and confirmed later in this study. These acceptor levels are designated Γ_8 and Γ_7 using the irreducible representations of the tetrahedral point group T_d . The level ordering is reversed in Fig. 2 compared to the usual energy diagram for electronic bands to represent the hole energy. The Γ_7 level is referred to as the split-off acceptor.

The electron of the acceptor-bound exciton resides in the conduction band, whereas two holes are located either at the Γ_8 or Γ_7 acceptor level. Therefore, the two-hole states of $\Gamma_8 \otimes \Gamma_8$, $\Gamma_7 \otimes \Gamma_8$, and $\Gamma_7 \otimes \Gamma_7$ symmetries can arise from low to high energies [Fig. 2(b)], where the symbol \otimes denotes the direct product of two irreducible representations. The splitting of the two-hole states by symmetry-breaking interactions is derived by treating the two holes quantum mechanically. We let \hat{j}_1 and \hat{j}_2 be the angular

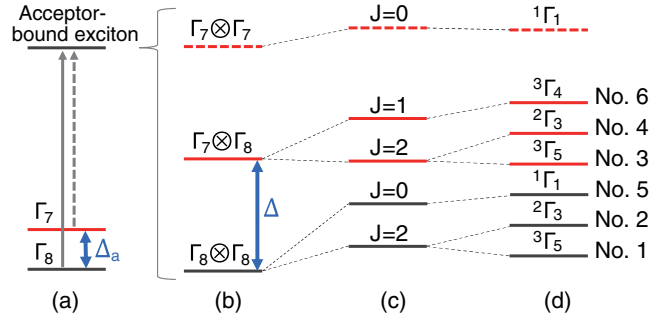


FIG. 2. (a) Schematic of absorption transitions from acceptor (Γ_8 , Γ_7) to acceptor-bound exciton states. (b) Two-hole states extended for split-off (Γ_7) holes, including (c) hole-hole exchange interaction and (d) crystal-field splitting. Δ_a and Δ denote the spin-orbit splitting in the acceptor and bound exciton states, respectively. The split levels are shown not to scale and grouped in (d) by the triplet system, rather than energy ordering (numbers 1–6) in the measured spectra.

momentum operators for the holes; $j_1, j_2 = 3/2$ (or $1/2$) correspond to the Γ_8 (or Γ_7 , split-off) acceptor levels. Similarly, $\hat{J} = \hat{j}_1 + \hat{j}_2$ is the total angular momentum operator of the two-hole state. The coupling of \hat{j}_1 and \hat{j}_2 yields $J = (3), 2, (1), 0$ as derived from $\Gamma_8 \otimes \Gamma_8$, $J = 2, 1$ from $\Gamma_7 \otimes \Gamma_8$, and $J = (1), 0$ from $\Gamma_7 \otimes \Gamma_7$. The levels in parentheses are states of two identical fermions sharing the same angular momentum state, which are forbidden by Pauli’s exclusion principle and therefore omitted in Fig. 2(c). The two-hole states range from low to high energies according to Hund’s rule in atomic theory [35]. There are two $J = 2$ states, and each splits into a doublet denoted by ${}^3\Gamma_5$ and ${}^2\Gamma_3$ under the T_d symmetry of the crystal field [Fig. 2(d)]. Here, the superscripts represent the dimension of the irreducible representations, that is, the degeneracy of the states. These level degeneracies were provisionally considered to indicate the absorption intensities in our level assignments in Table I.

To summarize the theory at this stage, we expect seven levels for acceptor-bound excitons. The fine structure in diamond is fundamentally more intricate than that in silicon, in which only a triplet from $\Gamma_8 \otimes \Gamma_8$ two-hole states is expected [black lines in Fig. 2(d)]. Another triplet ($\Gamma_7 \otimes \Gamma_8$) and singlet ($\Gamma_7 \otimes \Gamma_7$) are our first predictions, including the split-off acceptor, as indicated by the solid and dashed red lines. To compare with experiments probing absorption transitions, as shown in Fig. 2(a), we indexed the levels by numbers 1–6 from low to high energies in the measured spectra.

Our strategy of measuring absorption is complementary to luminescence and allows the direct estimation of relative oscillator strengths from the absorption intensities [12] without thermal broadening. The sample and equipment details can be found in Refs. [31,36]. We additionally implemented a higher-resolution monochromator to achieve the best spectral resolution of 0.14 meV corresponding to a

TABLE I. Results of the fitting of the spectrum in Fig. 4(a) to Eq. (1), compared with theory. E_i , peak energy; ΔE_i , separation from E_1 ; w_i , Lorentzian width (FWHM deconvoluted from the spectral resolution); A_i , areal intensity; \tilde{A}_i , areal intensity relative to line number 6 taken as three; g , level degeneracy; S, irreducible representation of the two-hole states; J , total angular momentum; T; irreducible representations of the constituent hole states; \tilde{A}_i^* , relative oscillator strengths calculated using the interaction parameters extracted in Sec. III of the Supplemental Material [37].

Line no.	Experiment					Theory				
	E_i (eV)	ΔE_i (meV)	w_i (meV)	A_i [meV(cm) $^{-1}$]	\tilde{A}_i	g	S	J	T	\tilde{A}_i^*
6	5.3715	15.3	0.54	0.567	3	3	Γ_4	1	$\Gamma_7 \otimes \Gamma_8$	3
5	5.3700	13.8	0.59	0.132	0.70	}1	Γ_1	0	$\Gamma_8 \otimes \Gamma_8$	0.67
5'	5.3693	13.1	0.31	0.070	0.37					
4	5.3682	12.0	0.70	0.336	1.78	}2	Γ_3	2	$\Gamma_7 \otimes \Gamma_8$	2
4'	5.3679	11.7	0.03	0.024	0.13					
3	5.3674	11.2	0.36	0.562	2.98	}3	Γ_5	2	$\Gamma_7 \otimes \Gamma_8$	3
3'	5.3662	10.0	0.82	0.051	0.27					
2	5.3598	3.6	0.48	0.152	0.80	}2	Γ_3	2	$\Gamma_8 \otimes \Gamma_8$	1.50
2'	5.3586	2.4	2.58	0.100	0.53					
1''	5.3570	0.8	0.24	0.091	0.48	}3	Γ_5	2	$\Gamma_8 \otimes \Gamma_8$	0.33
1	5.3562	0	0.21	0.430	2.28					
1'	5.3550	-1.2	2.58	0.219	1.16					

sixfold improvement over our previous report [31]. Further details, including the elimination of interference fringes, chromatic aberration, and the background irrelevant to the bound excitons, are provided in Sec. I of the Supplemental Material [37].

The representative absorption spectra of boron-doped diamond at 6–160 K are presented in Fig. 3(a). The high-temperature spectrum resembles those reported for cathodoluminescence [28]. Figure 3(b) shows the temperature (T) variation of the full width at half maximum (FWHM) of the highest energy peak (after deconvoluted from the spectral resolution of detection) and a linear fit with 8.1 $\mu\text{eV}/\text{K}$. Figure 3(c) shows the energy shift δ of the same peak and a fit using $\delta(T) = -[a\theta / \exp(\theta/T) - 1]$ [26], where $a = 11.0 \mu\text{eV}/\text{K}$ and $\theta = 307 \text{ K}$. As indicated by the dashed lines in Fig. 3(a), some of the peaks diminish with decreasing temperatures. We attribute them to the absorption transitions from the upper (Γ_7) acceptor level, which confirms that $\Delta_a = 2 \text{ meV}$ (details in Sec. II of the Supplemental Material [37]).

A higher-resolution spectrum obtained at 2 K is shown in Fig. 4(a), where the line numbers are indicated at the bottom. At least five lines (numbers 1'', 4', 4, 5', 5) are additionally resolved from only four lines (numbers 1, 2, 3, 6) in our previous report [31]. We fit the spectrum with the sum of Voigt functions, that is, the sum of Lorentzian functions

$$\alpha_{\text{fit}}(E) = \sum_i \frac{A_i}{\pi} \frac{2w_i}{4(E - E_i)^2 + w_i^2}, \quad (1)$$

convoluted with a Gaussian function representing the spectral resolution of the detection system. After carefully examining the residual of the fit, three lines (numbers 1', 2', and 3') were further included to represent the weak components. Therefore, i denotes 1', 1, 1'', 2', 2, 3', 3, 4', 4, 5', 5, and 6. A_i , w_i , and E_i denote the areal intensity, FWHM, and position of the peak, respectively. The best-fit functions for each peak are shown by thin lines. A comparison of the sum (dotted red line) with the data

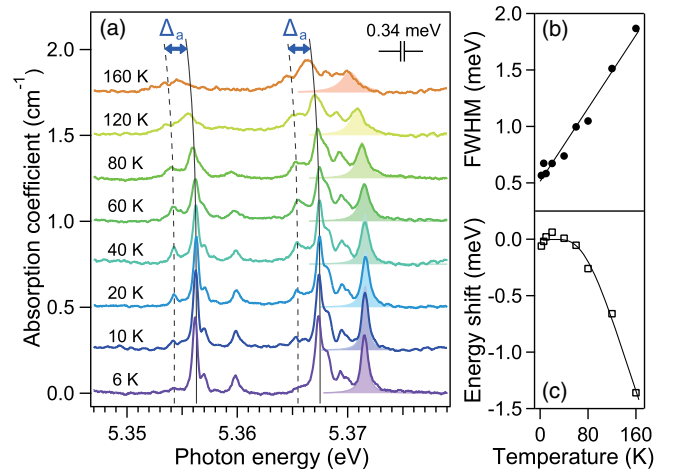


FIG. 3. (a) Absorption spectra of bound excitons in boron-doped diamond between 6 and 160 K. The dashed lines represent transitions from the upper acceptor level. (b) Temperature dependence of the Lorentzian width (FWHM) of line number 6 [shaded in (a)]. (c) Temperature shift of line number 6. The solid lines in (b) and (c) represent fit functions (see text).

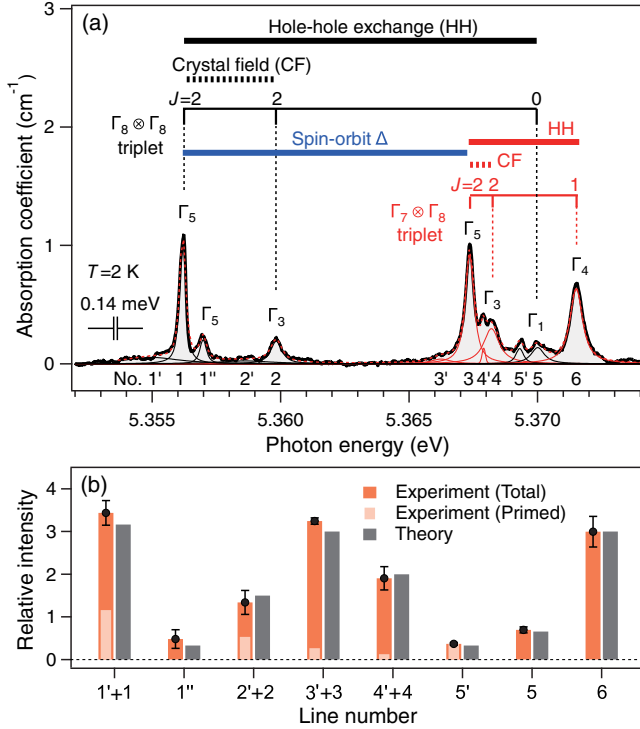


FIG. 4. (a) Higher-resolution absorption spectrum at 2 K (thick black line) fitted with the sum (dotted red line) of 11 Voigt functions, numbers 1'–6 (thin lines). The labels near the respective peaks represent the symmetry of the two-hole states. The brackets and horizontal bars at the top indicate two sets of triplets and the approximate size of the splittings, respectively. (b) Comparison of the experimental and theoretical absorption strengths. Orange bars with dots indicate the areal intensities of numbers 1, 2, and 4 superposed on top of numbers 1', 2', and 4', respectively. Thinner bars indicate intensities of primed peaks. The theory (gray bars) includes the electron-hole exchange effect for numbers 1'–2 and valley-orbit splitting for numbers 5' and 5 (details in Sec. III of the Supplemental Material [37]).

(thick black line) shows excellent agreement. The obtained fitting parameters are listed in Table I.

We attempted to assign the observed peaks to the respective bound-exciton levels by equating the intensities (\tilde{A}_i , obtained by normalizing A_i to a value of 3 for line number 6) with the level degeneracies (g). The results are summarized in Table I, which yields fair agreement between \tilde{A}_i and g . A more complete agreement is obtained by a model presented in Sec. III in the Supplemental Material [37] by introducing subsidiary interactions, such as electron-hole exchange. Although only numerical solutions were considered previously [13], we found that the total interaction Hamiltonian has analytical solutions. We derived the eigenvalues E_i^* and relative oscillator strength \tilde{A}_i^* of the dipole transitions using the atomic theory [35]. The theoretical strengths of numbers 1 and 2 were found to deviate from g , depending on the ratio of the electron-hole exchange to crystal-field interaction parameters. This

enabled the precise sizing of interaction parameters by fitting the measured spectrum to the analytically expressed $\alpha_{\text{fit}}(E)$ using E_i^* and \tilde{A}_i^* thus derived. The best-fit interaction parameters given in Table SIV of the Supplemental Material [37] yielded the theoretical strengths \tilde{A}_i^* (including those for some primed peaks) in Table I. The remarkable agreement with the experimental intensities \tilde{A}_i is presented in Fig. 4(b). This confirms the validity of our level assignments refined with the electron-hole exchange effect.

We observed that the fine structure follows the crystal-field scheme under the hole-hole exchange interaction [see horizontal bars in Fig. 4(a)]. The detailed attributions are as follows: Numbers 1, 2, and 5 constitute the $\Gamma_8 \otimes \Gamma_8$ triplet. Numbers 3, 4, and 6 constitute the $\Gamma_7 \otimes \Gamma_8$ (split-off) triplet, which was observed for the first time in cubic semiconductors. The transitions to the $\Gamma_7 \otimes \Gamma_7$ singlet were not observed despite the high sensitivity of our setup (see Fig. S3 in the Supplemental Material [37]). Numbers 2 (4) and 5 (6) lift from the ground state of the triplet mainly by the crystal-field splitting of 3.3 (0.9) meV and hole-hole exchange splitting of 12.3 (3.8) meV, respectively, whose effects have never been quantitatively discussed for diamond. The interdigitation of the two triplets, compared with Hund's rule, is explained by the large hole-hole exchange splitting in the $\Gamma_8 \otimes \Gamma_8$ triplet.

The minor splitting into lines of unprimed and primed numbers is considered two effects of coupling with the electron. Namely, we attribute the splitting of numbers 1 and 1'' to the electron-hole exchange interaction [13,45] and other splittings to weak valley-orbit coupling as seen in boron-doped silicon [46,47].

In luminescence studies [28,30], the insufficient spectral resolution owing to instrumental and thermal broadening (typically 1 meV) led to a confusing interpretation, attributing the separation between numbers 1 and 3 to the electron-hole exchange splitting of two identical internal structures. Our high-resolution absorption data excluded this possibility, and we further separated the size and primary origin of the internal splitting: $|E_2 - E_1| = 3.6$ meV by the crystal-field effect in the $\Gamma_8 \otimes \Gamma_8$ triplet, whereas $|E_6 - E_3| = 4.1$ meV by the hole-hole exchange in the $\Gamma_7 \otimes \Gamma_8$ triplet. The separation between the two triplets approximately provides the spin-orbit splitting. The refined value after removing the crystal-field and exchange energies by the least-squares fit was $\Delta = 14.3 \pm 0.1$ meV. This is the first accurate determination of the spin-orbit interaction parameter for acceptor-bound excitons in semiconductors. Consistent with the theoretical suggestions [48], this finding demonstrates that the spin-orbit splitting for the exciton complex in diamond is remarkably enhanced compared to that for the acceptor hole ($\Delta_a = 2$ meV).

We further examined previously reported observations [12–16,46,49–58] using our unified model and directly compared the extracted splitting of narrow- and wide-band-gap materials (Table SV, Supplemental Material [37]).

This provides the following general trends: (i) hole-hole exchange interactions dominate in cubic semiconductors, (ii) the $J = 2$ state forms the ground state of excitons bound to shallow acceptors, and (iii) diamond is an extreme case of large energy splitting among cubic semiconductors. The split-off hole appears owing to the high localization energy, which occurs similarly in wide-band-gap semiconductors of hexagonal structures. This confluent view including split-off hole bands addresses the gap in modeling exciton complexes in semiconductors.

In summary, we applied an analytical model developed for the interacting charges that form exciton complexes to the ultrafine splittings observed in the absorption spectra of boron-doped diamond. We explained the acceptor-bound exciton fine structure in diamond by two interdigitated triplets, thereby resolving a long-standing debate. The experimental confirmation of the lift of level degeneracies under external fields is an interesting future work. Highlighting the shared underlying physics among semiconductors, our findings may deepen understanding of the spin-orbit effects and symmetry breaking in systems such as nontrivial few-body bound states [4,20]. Our new knowledge of the fundamental properties of doped diamond also provides insights for future technologies beyond silicon, where excitons govern the optical properties at room temperature.

This work is partially supported by JSPS KAKENHI Grants No. JP22H01156 and No. JP17H02910, and PICS (Grant No. 200835) from Centre National de la Recherche Scientifique, France.

*naka@scphys.kyoto-u.ac.jp

- [1] L. Sun, L. Rademaker, D. Mauro, A. Scarfato, A. Psztor, I. Gutierrez-Lezama, Z. Wang, J. Martinez-Castro, A. F. Morpurgo, and C. Renner, Determining spin-orbit coupling in graphene by quasiparticle interference imaging, *Nat. Commun.* **14**, 3771 (2023).
- [2] S. Lee, H. Koike, M. Goto, S. Miwa, Y. Suzuki, N. Yamashita, R. Ohshima, E. Shigematsu, Y. Ando, and M. Shiraishi, Synthetic Rashba spin-orbit system using a silicon metal-oxide semiconductor, *Nat. Mater.* **20**, 1228 (2021).
- [3] G. I. Martone and N. Cherroret, Time translation symmetry breaking in an isolated spin-orbit-coupled fluid of light, *Phys. Rev. Lett.* **131**, 013803 (2023).
- [4] R. Liu, W. Wang, and X. Cui, Quartet superfluid in two-dimensional mass-imbalanced Fermi mixtures, *Phys. Rev. Lett.* **131**, 193401 (2023).
- [5] X. He, H. Htoon, S. K. Doorn, W. H. P. Pernice, F. Pyatkov, R. Krupke, A. Jeantet, Y. Chassagneux, and C. Voisin, Carbon nanotubes as emerging quantum-light sources, *Nat. Mater.* **17**, 663 (2018).
- [6] K. Zollner, M. Gmitra, and J. Fabian, Swapping exchange and spin-orbit coupling in 2D Van der Waals heterostructures, *Phys. Rev. Lett.* **125**, 196402 (2020).
- [7] D. Weinberg, Y. Park, D. T. Limmer, and E. Rabani, Size-dependent lattice symmetry breaking determines the exciton fine structure of perovskite nanocrystals, *Nano Lett.* **23**, 4997 (2023).
- [8] S. Ernst, P. J. Scheidegger, S. Diesch, L. Lorenzelli, and C. L. Degen, Temperature dependence of photoluminescence intensity and spin contrast in nitrogen-vacancy centers, *Phys. Rev. Lett.* **131**, 086903 (2023).
- [9] E. I. Rashba and G. E. Gurgenishvili, Edge absorption theory in semiconductors, *Sov. Phys. Solid State* **4**, 759 (1962).
- [10] H. Bethe and R. Peierls, Quantum theory of the dipton, *Proc. R. Soc. A* **148**, 146 (1935).
- [11] P. J. Dean and D. C. Herbert, Bound excitons in semiconductors, in *Excitons* (Springer, Berlin, 1979), pp. 55–182.
- [12] K. R. Elliott, G. C. Osbourn, D. L. Smith, and T. C. McGill, Bound-exciton absorption in Si:Al, Si:Ga, and Si:In, *Phys. Rev. B* **17**, 1808 (1978).
- [13] E. Molva and L. S. Dang, Magneto-optical study of Li and Na acceptor bound excitons in CdTe: Fine structure and cubic crystal-field effect, *Phys. Rev. B* **32**, 1156 (1985).
- [14] H. Mathieu, J. Camassel, and F. B. Chekroun, Stress effects on excitons bound to neutral acceptors in InP, *Phys. Rev. B* **29**, 3438 (1984).
- [15] M. Schmidt, T. N. Morgan, and W. Schairer, Stress effects on excitons bound to shallow acceptors in GaAs, *Phys. Rev. B* **11**, 5002 (1975).
- [16] B. Gil, P. Bigenwald, P. P. Paskov, and B. Monemar, Internal structure of acceptor-bound excitons in wide-band-gap wurtzite semiconductors, *Phys. Rev. B* **81**, 085211 (2010).
- [17] B. K. Meyer, J. Sann, S. Eisermann, S. Lautenschlaeger, M. R. Wagner, M. Kaiser, G. Callsen, J. S. Reparaz, and A. Hoffmann, Excited state properties of donor bound excitons in ZnO, *Phys. Rev. B* **82**, 115207 (2010).
- [18] G. Callsen, T. Kure, M. R. Wagner, R. Butté, and N. Grandjean, Excited states of neutral donor bound excitons in GaN, *J. Appl. Phys.* **123**, 215702 (2018).
- [19] G. Wang, A. Chernikov, M. M. Glazov, T. F. Heinz, X. Marie, T. Amand, and B. Urbaszek, Colloquium: Excitons in atomically thin transition metal dichalcogenides, *Rev. Mod. Phys.* **90**, 021001 (2018).
- [20] D. V. Tuan, S.-F. Shi, X. Xu, S. A. Crooker, and H. Dery, Six-body and eight-body exciton states in monolayer WSe₂, *Phys. Rev. Lett.* **129**, 076801 (2023).
- [21] T. Kazimierczuk, D. Fröhlich, S. Scheel, H. Stolz, and M. Bayer, Giant Rydberg excitons in the copper oxide Cu₂O, *Nature (London)* **514**, 343 (2014).
- [22] M. Assmann and M. Bayer, Semiconductor Rydberg physics, *Adv. Quantum Technol.* **3**, 1900134 (2020).
- [23] Y. Hazama, N. Naka, and H. Stolz, Mass-anisotropy splitting of indirect excitons in diamond, *Phys. Rev. B* **90**, 045209 (2014).
- [24] T. Ichii, N. Naka, and K. Tanaka, Rotational symmetry breaking on the Rydberg energy spectrum of indirect excitons in diamond studied by terahertz time-domain spectroscopy, *Phys. Rev. B* **104**, 205201 (2021).
- [25] C. D. Clark, P. J. Dean, and P. V. Harris, Intrinsic edge absorption in diamond, *Proc. R. Soc. A* **277**, 312 (1964).
- [26] K. Konishi and N. Naka, Phonon-assisted excitonic absorption in diamond, *Phys. Rev. B* **104**, 125204 (2021).

- [27] S. J. Sharp, A. T. Collins, G. Davies, and G. S. Joyce, Higher resolution studies of shallow bound exciton luminescence in diamond, *J. Phys. Condens. Matter* **9**, L451 (1997).
- [28] R. Sauer, H. Sternschulte, S. Wahl, K. Thonke, and T. R. Anthony, Revised fine splitting of excitons in diamond, *Phys. Rev. Lett.* **84**, 4172 (2000).
- [29] M. Cardona, T. Ruf, and J. Serrano, Comment on “Revised fine splitting of excitons in diamond,” *Phys. Rev. Lett.* **86**, 3923 (2001).
- [30] R. Sauer and K. Thonke, Sauer and Thonke reply, *Phys. Rev. Lett.* **86**, 3924 (2001).
- [31] Y. Kubo, S. Temgoua, R. Issaoui, J. Barjon, and N. Naka, Radiative lifetime of boron-bound excitons in diamond, *Appl. Phys. Lett.* **114**, 132104 (2019).
- [32] C. J. Rauch, Millimeter cyclotron resonance experiments in diamond, *Phys. Rev. Lett.* **7**, 83 (1961).
- [33] P. Y. Yu and M. Cardona, *Fundamentals of Semiconductors* (Springer, New York, 2010).
- [34] H. Kim, R. Vogelgesang, A. K. Ramdas, S. Rodriguez, M. Grimsditch, and T. R. Anthony, Electronic Raman and infrared spectra of acceptors in isotopically controlled diamonds, *Phys. Rev. B* **57**, 15315 (1998).
- [35] E. U. Condon and G. H. Shortley, *The Theory of Atomic Spectra* (Cambridge University Press, Cambridge, England, 1963).
- [36] R. Issaoui, J. Achard, A. Tallaire, F. Silva, A. Gicquel, R. Bisaro, B. Servet, G. Garry, and J. Barjon, Evaluation of freestanding boron-doped diamond grown by chemical vapour deposition as substrates for vertical power electronic devices, *Appl. Phys. Lett.* **100**, 122109 (2012).
- [37] See Supplemental Material at <http://link.aps.org/supplemental/10.1103/PhysRevLett.132.096902> for experimental details, temperature dependence, and a description of our theory, which includes Refs. [38–44].
- [38] D. G. Thomas and J. J. Hopfield, Optical properties of bound exciton complexes in cadmium sulfide, *Phys. Rev.* **128**, 2135 (1962).
- [39] S. Sugano, Y. Tanabe, and H. Kamimura, *Multiplets of Transition-Metal Ions in Crystals* (Academic Press, New York, 1970).
- [40] G. F. Koster, J. O. Dimmock, R. G. Wheeler, and H. Statz, *Properties of the Thirty-Two Point Groups* (MIT Press, Cambridge, MA, 1963).
- [41] T. Morgan, Oscillator strengths for electron-hole complexes (A^0X), *J. Phys. C* **10**, L131 (1977).
- [42] B. Hönerlage and I. Pelant, *Symmetry and Symmetry-Breaking in Semiconductors*, (Springer, New York, 2018).
- [43] Y. Kubo, M. Takahata, S. Temgoua, R. Issaoui, J. Barjon, and N. Naka, Phonon-assisted transitions of bound excitons in diamond: Analysis by mirror symmetry, *Phys. Rev. B* **101**, 205204 (2020).
- [44] P. J. Dean, W. F. Flood, and G. Kaminsky, Absorption due to bound excitons in silicon, *Phys. Rev.* **163**, 721 (1967).
- [45] G. E. Pikus and G. L. Bir, Exchange interaction in excitons in semiconductors, *Sov. Phys. JETP* **33**, 108 (1971).
- [46] V. A. Karasyuk, A. G. Steele, A. Mainwood, E. C. Lightowers, G. Davies, D. M. Brake, and M. L. W. Thewalt, Ultrahigh-resolution photoluminescence studies of excitons bound to boron in silicon under uniaxial stress, *Phys. Rev. B* **45**, 11736 (1992).
- [47] A. Yang, M. Steger, T. Sekiguchi, D. Karaiskaj, M. L. W. Thewalt, M. Cardona, K. M. Itoh, H. Riemann, N. V. Abrosimov, M. F. Churbanov, A. V. Gusev, A. D. Bulanov, I. D. Kovalev, A. K. Kaliteevskii, O. N. Godisov, P. Becker, H.-J. Pohl, J. W. Ager, and E. E. Haller, Single-frequency laser spectroscopy of the boron bound exciton in ^{28}Si , *Phys. Rev. B* **80**, 195203 (2009).
- [48] J. Serrano, M. Cardona, and T. Ruf, Spin-orbit splitting in diamond: Excitons and acceptor related states, *Solid State Commun.* **113**, 411 (1999).
- [49] O. Madelung, *Semiconductors: Data Handbook* (Springer, New York, 2004).
- [50] T. Shimomura, Y. Kubo, J. Barjon, N. Tokuda, I. Akimoto, and N. Naka, Quantitative relevance of substitutional impurities to carrier dynamics in diamond, *Phys. Rev. Mater.* **2**, 094601 (2018).
- [51] A. Baldereschi and N. O. Lipari, Spherical model of shallow acceptor states in semiconductors, *Phys. Rev. B* **8**, 2697 (1973).
- [52] J. Barjon, Luminescence spectroscopy of bound excitons in diamond, *Phys. Status Solidi A* **214**, 1700402 (2017).
- [53] M. Vouk and E. Lightowers, A high resolution investigation of the recombination radiation from Si containing the acceptors B, Al, Ga, In and Tl, *J. Lumin.* **15**, 357 (1977).
- [54] Y. Takeuchi, Y. Makita, K. Kudo, T. Nomura, H. Tanaka, K. Irie, and N. Ohnishi, Observation of new common emissions in GaAs produced by ion implantation of four acceptor impurities, *Appl. Phys. Lett.* **48**, 59 (1986).
- [55] J. Gutowski, Electronic and vibronic states of the acceptor-bound-exciton complex (A^0, X) in CdS. II. Determination of the fine structure of the (A^0, X_B) electronic states by high-resolution excitation spectroscopy, *Phys. Rev. B* **31**, 3611 (1985).
- [56] A. Wyszomolek, M. Potemski, R. Stepniewski, J. Lusakowski, K. Pakula, J. M. Baranowski, J. Martinez, P. Wyder, I. Grzegory, and S. Porowski, Polarised magnetoluminescence of excitons in homoepitaxial GaN layers, *Phys. Status Solidi B* **216**, 11 (1999).
- [57] R. Ishii, A. Yoshikawa, M. Funato, and Y. Kawakami, Revisiting the substitutional Mg acceptor binding energy of AlN, *Phys. Rev. B* **108**, 035205 (2023).
- [58] T. Karin, R. J. Barbour, C. Santori, Y. Yamamoto, Y. Hirayama, and Kai-Mei C. Fu, Radiative properties of multicarrier bound excitons in GaAs, *Phys. Rev. B* **91**, 165204 (2015).